# High-Speed MSM/HEMT and p-i-n/HEMT Monolithic Photoreceivers

P. Fay, *Member, IEEE*, C. Caneau, and I. Adesida, *Fellow, IEEE*

***Abstract*—The performance of monolithically integrated metal–semiconductor–metal/high electron-mobility transistor (MSM/HEMT) and p-i-n/HEMT photoreceivers is reported. p-i-n/HEMT photoreceivers have been designed and fabricated, resulting in measured transimpedances of 700 Ω, an 8.3-GHz bandwidth, and measured sensitivities of −17.7 dBm at 10 Gb/s and −15.8 dBm at 12 Gb/s for a $2^{31}-1$ pattern length pseudorandom bit sequence at a bit error rate of $10^{-9}$. Low-noise MSM-based photoreceivers have also been designed and fabricated, and frequency response, noise, and sensitivity measurements have been performed. Sensitivities of −16.9, −13.1, and −10.7 dBm were obtained at 5, 8, and 10 Gb/s, respectively. A direct comparison of p-i-n– and MSM-based photoreceivers is undertaken on photoreceivers with matched responsivity and bandwidth. Measurement and theoretical analysis of circuit and device noise indicates an anomalous sensitivity penalty in MSM-based receivers that arises due to intersymbol interference.**

***Index Terms*—MSM photodetectors, optoelectronic integrated circuits, photoreceivers, p-i-n photodiodes.**

## I. Introduction

As DATA RATES in fiber telecommunications systems continue to increase, low-noise photoreceivers capable of operating at very high speeds are required. In order to maximize the speed of a photoreceiver front end, minimization and careful control of the interconnect parasitics between the photodetector and electrical amplifier are essential. One attractive approach for controlling and reducing these interconnect parasitics is to monolithically integrate the photodetector with active electrical devices for amplification and signal processing on a common substrate. The viability of this approach has been established for photoreceivers based on p-i-n photodiodes, with demonstrations of sensitivities better than −17 dBm at data rates of 20 Gb/s [1] and bandwidths as high as 46.5 GHz [2]. 40-Gb/s operation has also recently been demonstrated [2]–[4]. Although most efforts in high-speed photoreceivers to date have used p-i-n photodiodes, metal–semiconductor–metal (MSM) photodetectors are an alternative that may offer possible advantages due to the inherently low capacitance of the interdigitated electrode geometry [5]. The low capacitance/area of the MSM allows a larger area detector to be used while maintaining adequate bandwidth, easing fiber alignment tolerances and reducing packaging complexity. Alternatively, the low MSM photodetector capacitance may also be useful for achieving higher data rates.

The design, fabrication, and characterization of low-noise monolithically integrated photoreceivers based on both MSMs and p-i-n photodiodes coupled with high electron-mobility transistors (HEMTs) on InP substrates are described. The photoreceivers have been characterized using small-signal

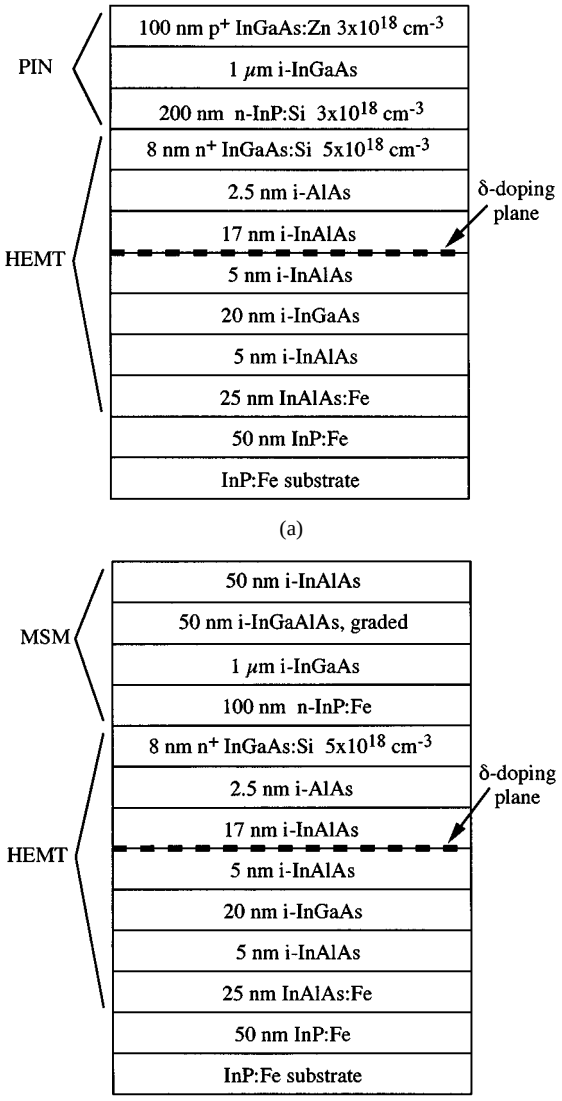


Fig. 1. Heterostructures for monolithically integrated: (a) p-i-n/HEMT and (b) MSM/HEMT photoreceivers.

Manuscript received May 17, 2000; revised March 21, 2001. This work was supported by the National Science Foundation under Grant ECD 89-43166 and by the Advanced Research Projects Agency under Grant MDA 972-941-0004.

P. Fay is with the Department of Electrical Engineering, University of Notre Dame, Notre Dame, IN 46556 USA (e-mail: pfay@nd.edu).

C. Caneau is with Corning Inc., Corning, NY 14831 USA.

I. Adesida is with the Department of Electrical and Computer Engineering, Microelectronics Laboratory, University of Illinois at Urbana-Champaign, Urbana, IL 61801 USA.

Publisher Item Identifier S 0018-9480(02)00761-5.

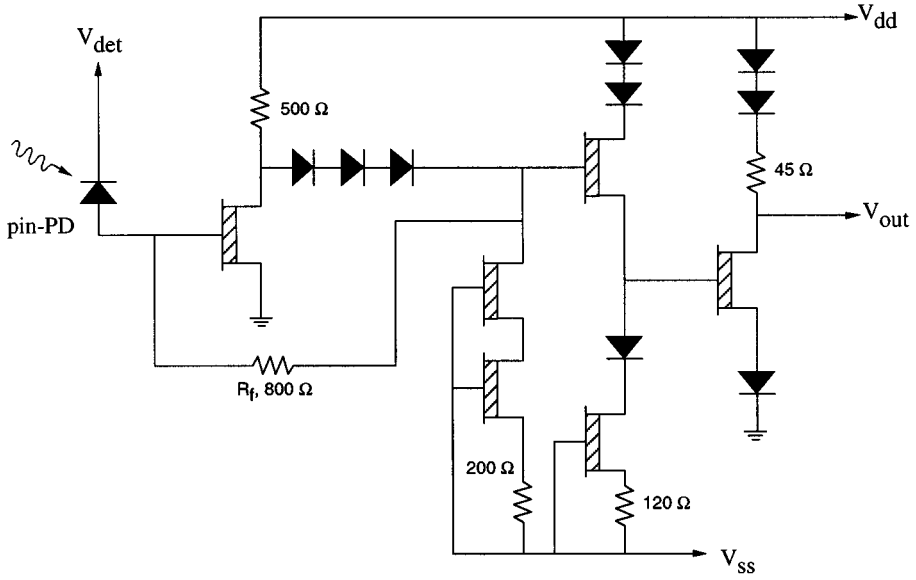


Fig. 2. Circuit schematic diagram for a high-speed low-noise p-i-n/HEMT photoreceiver.

frequency response and noise spectral-density measurements, as well as by bit error rate (BER) characterization of packaged photoreceiver modules at data rates of up to 12 Gb/s. Experimental results are presented and the results obtained for MSM- and p-i-n-based circuits are compared to each other and to theoretical expectations.

## II. Integration and Fabrication Technology

For the photoreceivers discussed in this paper, the integration of photodetector and HEMT was implemented using a stacked layer structure in which the HEMT was grown first, followed by a barrier layer and the photodetector (either p-i-n or MSM). The general framework of a stacked layer structure was selected for its relative simplicity in heterostructure growth. Cross-sectional diagrams of the complete p-i-n/HEMT and MSM/HEMT heterostructures are shown in Fig. 1(a) and (b), respectively. For both MSM- and p-i-n-based structures, an InP barrier has been inserted between the HEMT cap and the bottom of the photodetector. This serves both to electrically isolate the photodetector absorption region from the underlying HEMT layers, as well as to provide a robust etch stop layer for ease of fabrication [6]. Both the p-i-n- and MSM-based heterostructures were grown using organometallic vapor-phase epitaxy (OMVPE), and both structures were grown on unpatterned substrates in single uninterrupted growth runs.

The circuits were fabricated using a mix-and-match optical lithography and electron-beam lithography process. Device isolation for both the photodetectors and the HEMTs was accomplished using sequential selective wet chemical etching. Mushroom-shaped gates with a gate length of 0.2- and 0.5-$\mu$m-wide MSM electrodes were defined using electron beam lithography and liftoff of evaporated TiAu metallization. Plasma-enhanced chemical vapor deposition (PECVD) $SiN_x$ was used to form dielectric crossovers, metal–insulator–metal capacitors, passivation, and antireflection coatings. Discrete HEMTs fabricated on both the MSM/HEMT and p-i-n/HEMT heterostructures exhibited nearly identical behavior. Excellent dc and microwave performance was achieved, with peak transconductances of over 800 mS/mm and threshold voltages of $-0.7$ V. On-wafer high-frequency characterization demonstrated $f_t$'s of over 115 GHz and $f_{\max}$'s in excess of 150 GHz.

## III. p-i-n-Based Photoreceivers

The p-i-n/HEMT photoreceivers were fabricated using the heterostructure shown in Fig. 1(a). A normal-incidence p-i-n photodiode with an absorption layer thickness of 1 $\mu$m was selected as a compromise between high quantum efficiency, short photocarrier transit time, and small device capacitance. The photoreceiver preamplifier has been designed to take advantage of the low-noise high-speed performance attainable with submicrometer gate-length HEMTs. The circuit schematic of a high-speed p-i-n/HEMT photoreceiver is shown in Fig. 2. A three-stage transimpedance amplifier topology based on feedback regulation of the first-stage gain and a source-degenerated low-gain final stage was used. This final stage, in addition to providing a small amount of additional voltage gain, also provides output impedance matching to 50 $\Omega$. A broad-band output match is achieved with this circuit, with an output voltage standing-wave ratio (VSWR) of less than 1.35 for frequencies up to 18 GHz. The biasing conditions for all HEMTs in the main signal path have been chosen for low-noise operation.

The photoreceivers were characterized for small-signal performance, as well as for large-signal digital performance. The small-signal optoelectronic frequency response for 1.55-$\mu$m wavelength light and the input-referred noise current spectral density are shown in Fig. 3. The 3-dB bandwidth of the circuit is 8.3 GHz, and is limited by the bandwidth of the electrical amplifier. The measured receiver responsivity is 410 V/W into a 50-$\Omega$ load. Measurements of discrete photodiodes on the

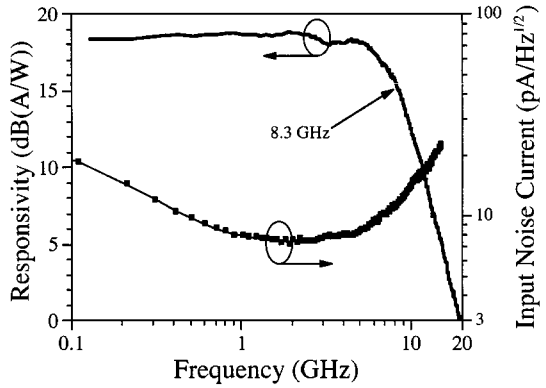


Fig. 3. Optoelectronic frequency response and input-referred noise current spectral density. The measured $-3$ dB bandwidth is 8.3 GHz with a low-frequency responsivity of 410 V/W. The average input-referred noise current density of 8.8 pA/Hz$^{1/2}$ is obtained from 300 MHz to 8.3 GHz.

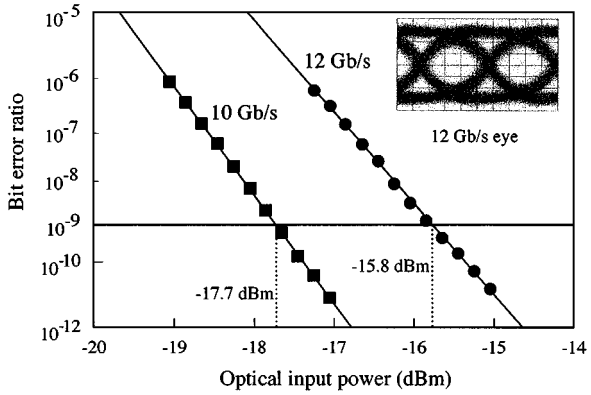


Fig. 4. BER performance of p-i-n/HEMT photoreceivers at 10 and 12 Gb/s. Sensitivities of $-17.7$ and $-15.8$ dBm are obtained for $2^{31}-1$ pattern length PRBS. Inset: eye pattern at 12 Gb/s.

same wafer as the photoreceivers indicates that the photodiodes have responsivities of 0.58 A/W, corresponding to an external quantum efficiency of 47%. The midband transimpedance of the photoreceiver's electrical amplifier, including the effects of loading by the photodetector, is 700 $\Omega$. The input-referred noise current spectral density shown in Fig. 3 was obtained from the measured output noise power spectrum (with no optical input present) and the measured frequency response. The photoreceiver exhibited an average input noise current spectral density of 8.8 pA/Hz$^{1/2}$ over the frequency range from 300 MHz to 8.3 GHz.

The noise performance of the photoreceiver for digital applications was also assessed at 10 and 12 Gb/s [7]. Fig. 4 shows the BER performance of a packaged photoreceiver module at 10 and 12 Gb/s with the obtained eye diagram at 12 Gb/s as an inset. For a $2^{31}-1$ pattern length pseudorandom bit sequence (PRBS), the measured sensitivities were $-17.7$ dBm at 10 Gb/s and $-15.8$ dBm at 12 Gb/s for a BER of $10^{-9}$. These sensitivities are within 0.7 dB of those predicted from circuit simulation considering the measured noise parameters of the HEMTs, room-temperature thermal noise in the resistors, and the shot noise arising from the photodetector dark current.

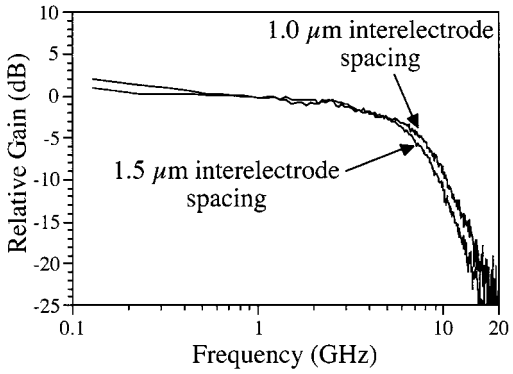


Fig. 5. Optoelectronic frequency response for MSM/HEMT photoreceivers with 1.0- and 1.5-$\mu$m interelectrode spacings. 7.2-GHz bandwidth is obtained for 1.0-$\mu$m spacing, while 5.6 GHz is obtained for a 1.5-$\mu$m interelectrode spacing.

## IV. MSM-Based Photoreceivers

MSM-based photoreceivers were fabricated using the heterostructure illustrated in Fig. 1(b). The MSM portion of the heterostructure consists of a 100-nm InP : Fe barrier layer, a 1-$\mu$m–thick undoped InGaAs absorption region, 50 nm of undoped compositionally graded InGaAlAs, and 50 nm of undoped InAlAs for the MSM Schottky contacts. The graded layer between the absorption and Schottky layers is designed to eliminate conduction- and valence-band offsets that can impede photocarrier transport and collection by the electrodes. The HEMT portion of the heterostructure is identical to that used in the p-i-n/HEMT circuits, and nearly identical device performance was achieved.

MSM-based photoreceivers using a three-stage transimpedance amplifier similar to that used for the p-i-n/HEMT photoreceivers were designed and fabricated [8]. The small-signal frequency response of the photoreceivers was characterized on-wafer at a wavelength of 1.55 $\mu$m. Fig. 5 shows the frequency responses obtained for two slightly different MSM/HEMT photoreceiver designs. A bandwidth of 7.2 GHz was obtained for a photoreceiver containing an MSM with a 1.0-$\mu$m interelectrode spacing, while a bandwidth of 5.6 GHz was measured for a photoreceiver containing an MSM with a 1.5-$\mu$m interelectrode spacing. The receiver responsivity into a 50-$\Omega$ load was measured to be 242- and 273-V/W for receivers with 1.0- and 1.5-$\mu$m interelectrode spacings, respectively. Discrete MSMs had measured responsivities of 0.32 and 0.36 A/W for 1.0- and 1.5-$\mu$m interelectrode spacings, respectively, in good agreement with theoretical expectations.

Direct measurement of BERs of packaged MSM-based photoreceiver modules was also performed; Fig. 6 shows the BER performance of the MSM/HEMT photoreceivers at 5, 8, and 10 Gb/s. The 5- and 8-Gb/s results are for a photoreceiver with a 1.5-$\mu$m interelectrode spacing, while the 10-Gb/s results were obtained using a photoreceiver with a 1-$\mu$m interelectrode spacing in order to achieve a sufficiently large bandwidth. Sensitivities of $-16.9$, $-13.1$, and $-10.7$ dBm were obtained for a $2^7-1$ pattern length PRBS and a BER of $10^{-9}$ at 5, 8, and 10 Gb/s, respectively.

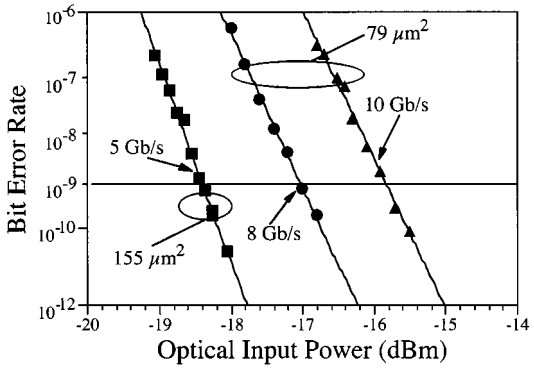


Fig. 6. BER performance at 5, 8, and 10 Gb/s for integrated MSM/HEMT photoreceivers. Sensitivities are −16.9, −13.1, and −10.7 dBm for bit rates of 5, 8, and 10 Gb/s, respectively.

## V. MSM- AND p-i-n-BASED PHOTORECEIVER COMPARISON

To facilitate comparison of these two monolithic receiver technologies, MSM- and p-i-n-based photoreceivers specifically designed to have nearly identical bandwidth and responsivity characteristics were fabricated and tested. In order to achieve approximately the same overall receiver responsivity for both the p-i-n- and MSM-based photoreceivers, the preamplifier's feedback resistor was chosen to be 800 Ω for the MSM/HEMT receivers and 500 Ω for the p-i-n/HEMT devices; the amplifiers are otherwise identical. Selection of this ratio compensates for the experimentally observed difference in responsivity between the two detector types. To achieve equal photoreceiver bandwidths with each detector type, the photodetector areas have also been scaled. Due to the much lower capacitance per area of the MSM photodetector, this translates into a considerably larger MSM than p-i-n photodiode. The scaling of the amplifier transimpedance, however, reduces the required detector areal ratio by broadening the bandwidth of the p-i-n/HEMT electrical preamplifier relative to the MSM/HEMT version. The MSMs used had an area of $(25\ \mu\text{m})^2$, with 0.5-$\mu$m-wide electrodes and either a 1.0- or 1.5-$\mu$m interelectrode spacing. For comparable photoreceiver bandwidths, circular p-i-n photodiodes with areas of 79 and 155 $\mu\text{m}^2$, respectively, were used, with responsivities of 0.47 and 0.53 A/W when coupled using a lensed fiber. The difference in responsivity between the two p-i-n photodiodes is due to incomplete optical coupling into the smaller detector. The p-i-n/HEMT receiver with a 79-$\mu\text{m}^2$-area detector was designed to have the same bandwidth as the receiver with a 1-$\mu$m interelectrode gap MSM. Although an MSM with a 1.5-$\mu$m interelectrode spacing has a much lower capacitance than a 155-$\mu\text{m}^2$ area p-i-n, this MSM geometry is transit-time limited while the p-i-n photodiode is not and, thus, a disproportionally larger p-i-n–photodiode capacitance is required to equalize the receiver bandwidths.

The bandwidth of the p-i-n/HEMT photoreceivers was found to be 7.5 and 5.6 GHz for the 79- and 155-$\mu\text{m}^2$ detector areas, respectively, compared to 7.2 and 5.6 GHz for the 1.0- and 1.5-$\mu$m spacing MSM/HEMT photoreceivers. This shows that these MSM/HEMT and p-i-n/HEMT photoreceivers are well matched in terms of bandwidth, and that both are suitable for operation to 10 Gb/s and above. The measured responsivity of the p-i-n/HEMT photoreceivers was 248 V/W into a 50-Ω load for a photoreceiver with a 155-$\mu\text{m}^2$ detector, and 220 V/W for the 79-$\mu\text{m}^2$ detector, compared to 273 and 242 V/W for the 1.5- and 1.0-$\mu$m MSM photoreceivers, indicating that the responsivity of the MSM- and p-i-n-based receivers are also comparable. The difference in responsivities in the case of the p-i-n-based receivers is due to imperfect coupling of the incident light from the fiber probe into the small-area detectors, while for the MSM-based circuits, this is due to the increase in external quantum efficiency for MSMs with larger interelectrode spacings.

The BER performance of these responsivity-bandwidth matched p-i-n/HEMT photoreceivers was investigated. Sensitivities of −18.4, −17.0, and −15.8 dBm were obtained at 5, 8, and 10 Gb/s, respectively. A photoreceiver with a 155-$\mu\text{m}^2$ photodetector was used for the 5-Gb/s data, while the higher speed BER results were obtained using a photoreceiver with a 79-$\mu\text{m}^2$ photodetector. For the comparable MSM/HEMT photoreceivers, the measured sensitivities were −16.9, −13.1, and −10.7 dBm at 5, 8, and 10 Gb/s.

A simple system analysis that considers only bit errors due to noise and limited receiver bandwidth results in the following expression for photoreceiver sensitivity:

$$\bar{P} = \frac{\text{SNR}}{2 \cdot \Re}\sqrt{\langle i_c^2 \rangle}\left[1 - 2\exp\left(-\frac{\pi f_{3\text{ dB}}}{B}\right)\right]^{-1} \qquad (1)$$

where $B$ is the bit rate, $f_{3\text{ dB}}$ is the photoreceiver bandwidth, $\Re$ is the photodetector responsivity, SNR is the required signal-to-noise ratio for operation at the desired bit-error ratio ($\text{SNR} = 12$ for $\text{BER} = 10^{-9}$), and $\bar{P}$ is the sensitivity. The total input-referred noise current in this expression includes both detector and amplifier noise contributions and is given by $\langle i_c^2 \rangle = \left\langle i_{\text{pd}}^2 \right\rangle + \langle i_{\text{amp}}^2 \rangle$, where $\left\langle i_{\text{pd}}^2 \right\rangle = (2qI_{\text{pd}} + (kT/R_{\text{pd}})) \cdot \Delta f$ is the shot and thermal noise contributions of the photodetector, and $\left\langle i_{\text{amp}}^2 \right\rangle$ is the input-referred noise current of the transimpedance amplifier. From this simple analysis, the p-i-n/HEMT receivers should exhibit a 1.25-dB improvement in sensitivity over the 1.5-$\mu$m interelectrode spacing MSM/HEMT receivers and a 1.76-dB improvement over comparable 1-$\mu$m interelectrode spacing MSM/HEMT photoreceivers due to the p-i-n photodiode's superior responsivity if the input noise current is the same for both photoreceivers. The experimentally observed difference in sensitivity, however, favors the p-i-n/HEMT designs by considerably larger margins than this simple analysis suggests. In fact, the p-i-n/HEMT receiver sensitivity is found to be superior to the MSM/HEMT receiver sensitivity by 1.5 dB at 5 Gb/s, 3.9 dB at 8 Gb/s, and 5.1 dB at 10 Gb/s. To investigate experimentally the source of this discrepancy, the input noise current spectral density for both types of receivers was determined from on-wafer measurements of output noise power without an optical signal present. For the MSM/HEMT receivers, an average input-referred noise current of 6.5 $\text{pA/Hz}^{1/2}$ was obtained for an MSM/HEMT receiver with a 1-$\mu$m interelectrode gap, while 7.3 $\text{pA/Hz}^{1/2}$ was obtained for a receiver with a 1.5-$\mu$m interelectrode gap. For the p-i-n/HEMT photoreceivers, the average input noise current spectral density was found to be 11.4 $\text{pA/Hz}^{1/2}$ for

TABLE I
SUMMARY OF SENSITIVITY COMPUTED FROM INPUT NOISE CURRENT AND MEASURED SENSITIVITY FOR MSM/HEMT AND p-i-n/HEMT PHOTORECEIVERS

| Bit Rate (Gb/s) | MSM/HEMT | | PIN/HEMT | |
|---|---|---|---|---|
| | From noise current (dBm) | Direct measurement (dBm) | From noise current (dBm) | Direct measurement (dBm) |
| 5 | -19.1 | -16.9 | -19.2 | -18.4 |
| 8 | -17.3 | -13.1 | -17.0 | -17.0 |
| 10 | -15.8 | -10.7 | -15.5 | -15.8 |

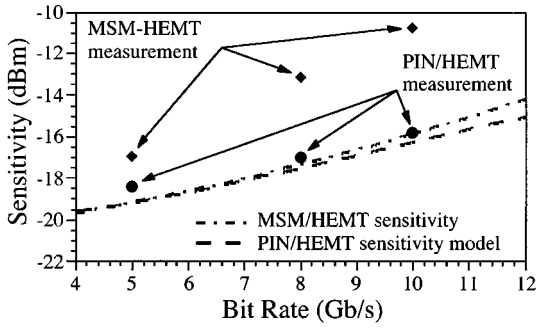


Fig. 7. Directly measured sensitivity and noise-measurement-based sensitivity model estimates versus BER for MSM/HEMT and p-i-n/HEMT photoreceivers.

both the 79- and 155-$\mu$m$^2$–area detectors. The higher input noise current densities of these p-i-n-based receivers compared to the MSM versions is due to a combination of the larger dark current of these p-i-n photodiodes, as well as the lower gain (but comparable additive amplifier noise) of the electrical preamplifiers for the p-i-n-based circuits. Increased amplifier noise is expected for the responsivity-bandwidth matched p-i-n/HEMT circuits fabricated here since the input noise current of a shunt–shunt feedback transimpedance amplifier is given approximately by $\langle i_{\rm amp}^2 \rangle = \langle i_{\rm ol}^2 \rangle + (4kT\Delta f/R_f)$, where $\langle i_{\rm ol}^2 \rangle$ is the noise current of the open-loop amplifier and $R_f$ is the feedback resistance. As the amplifiers are identical, except for the value of the feedback resistance, $\langle i_{\rm ol}^2 \rangle$ is the same for both the MSM and p-i-n photoreceivers. From the second term in the amplifier noise expression, however, the amplifier noise contribution decreases with increasing feedback resistance. Since the transimpedance (and thus the feedback resistance) was reduced in the p-i-n/HEMT circuits relative to the MSM-based circuits, the amplifier current noise in the p-i-n circuits is expected to be larger. This is verified experimentally by the larger measured noise current spectral densities of the p-i-n/HEMT receivers compared to the MSM/HEMT receivers. Despite this disadvantage of increased amplifier noise in the p-i-n/HEMT receivers, the measured sensitivities are considerably better than those obtained for the MSM/HEMT devices. A summary of the sensitivities computed from these measured input noise current spectra and the directly measured sensitivity for selected bit rates is presented in Table I. Fig. 7 shows the measured sensitivities, as well as the sensitivities estimated from noise measurements using the model shown in (1) for both the MSM/HEMT and p-i-n/HEMT photoreceivers. For the p-i-n/HEMT photoreceivers, the directly measured sensitivities follow the same trend and are within 0.8 dB of the values obtained from the input-referred noise currents and match the simple noise model quite well, indicating that this model adequately describes the performance of the photoreceivers and that detector and amplifier noise is the dominant source of bit errors. For the MSM/HEMT photoreceivers, however, substantial discrepancies exist between the predictions based on noise current spectral-density measurements and the direct digital BER sensitivity measurements. This deviation indicates that bit errors caused by intersymbol interference significantly degrade the performance of the MSM-based photoreceivers at higher bit rates, while no such effect is observed for the p-i-n-based receivers.

## VI. CONCLUSIONS

The design, fabrication, and low-noise performance of monolithically integrated MSM/HEMT and p-i-n/HEMT photoreceivers have been described. Sensitivities of $-17.7$ and $-15.8$ dBm have been achieved for p-i-n/HEMT receivers at 10 and 12 Gb/s, respectively, for $2^{31}-1$ length PRBS data sequences. Responsivity-bandwidth matched p-i-n/HEMT and MSM/HEMT receivers have been fabricated to facilitate comparison of achievable performance with the two photoreceiver technologies. The electrical amplifier transimpedance and the photodetector areas have been scaled to result in nearly identical photoreceiver bandwidths and responsivities. Sensitivity measurements of the responsivity-bandwidth matched p-i-n/HEMT and MSM/HEMT receivers indicate that the p-i-n-based circuits enjoy an advantage of 1.5, 3.9, and 5.1 dB at 5, 8, and 10 Gb/s, respectively. The noise performance of the photoreceivers has been assessed, and sensitivity limits due to the measured noise were determined. The p-i-n/HEMT circuits were found to be noise limited, while the BER in MSM/HEMT circuits is limited by both noise and intersymbol interference.

## ACKNOWLEDGMENT

The authors gratefully acknowledge the assistance of M. Arafa, Intel Corporation, Portland, OR, S. Chandrasekhar, Lucent Technologies, Holmdel, NJ, L. Lunardi, JDS Uniphase, Freehold, NJ, and W. Wohlmuth, TriQuint Semiconductor, Hillsboro, OR, for valuable assistance and discussions.

## REFERENCES

[1] L. M. Lunardi, S. Chandrasekhar, A. H. Gnauck, and C. A. Burrus, "20-Gb/s monolithic p–i–n/HBT photoreceiver module for 1.55-$\mu$m applications," *IEEE Photon. Technol. Lett.*, vol. 7, pp. 1201–1203, Oct. 1995.

[2] K. Takahata, Y. Muramoto, H. Fukano, K. Kato, A. Kozen, O. Nakajima, and Y. Matsuoka, "46.5 GHz-bandwidth monolithic receiver OEIC consisting of a waveguide p–i–n photodiode and a HEMT distributed preamplifier," *IEEE Photon. Technol. Lett.*, vol. 10, pp. 1150–1152, Aug. 1998.

[3] M. Bitter, R. Bauknecht, W. Hunziker, and H. Melchior, "Monolithic InGaAs–InP p–i–n/HBT 40-Gb/s optical receiver module," *IEEE Photon. Technol. Lett.*, vol. 12, pp. 74–76, Jan. 2000.
[4] K. Takahata, Y. Muramoto, H. Fukano, K. Kato, A. Kozen, S. Kimura, Y. Imai, Y. Miyamoto, O. Nakajima, and Y. Matsuoka, "Ultrafast monolithic receiver OEIC composed of multimode waveguide p–i–n photodiode and HEMT distributed amplifier," *IEEE J. Select. Topics Quantum Electron.*, vol. 6, pp. 31–37, Jan. 2000.
[5] J. D. B. Soole and H. Schumacher, "InGaAs metal–semiconductor–metal photodetectors for long wavelength optical communications," *IEEE J. Quantum Electron.*, vol. 27, pp. 737–752, Mar. 1991.
[6] P. Fay, M. Arafa, W. A. Wohlmuth, C. Caneau, S. Chandrasekhar, and I. Adesida, "Design, fabrication, and performance of high-speed monolithically integrated InAlAs/InGaAs/InP MSM/HEMT photoreceivers," *J. Lightwave Technol.*, vol. 15, pp. 1871–1879, Oct. 1997.
[7] P. Fay, W. Wohlmuth, A. Mahajan, C. Caneau, S. Chandrasekhar, and I. Adesida, "Low-noise performance of monolithically integrated 12-Gb/s p–i–n/HEMT photoreceiver for long-wavelength transmission systems," *IEEE Photon. Technol. Lett.*, vol. 10, pp. 713–715, May 1998.
[8] P. Fay, W. Wohlmuth, C. Caneau, S. Chandrasekhar, and I. Adesida, "High-speed digital and analog performance of low-noise integrated MSM–HEMT photoreceivers," *IEEE Photon. Technol. Lett.*, vol. 9, pp. 991–993, July 1997.

**P. Fay** (S'89–M'91) received the B.S. degree in electrical engineering from the University of Notre Dame, Notre Dame, IN, in 1991, and the M.S. and Ph.D. degrees in electrical engineering from the University of Illinois at Urbana-Champaign, in 1993 and 1996, respectively.

From 1992 to 1994, he was a National Science Foundation Graduate Research Fellow, and a Visiting Assistant Professor in the Department of Electrical and Computer Engineering, University of Illinois at Urbana-Champaign, in 1996 and 1997. He is currently an Assistant Professor in the Department of Electrical Engineering, University of Notre Dame. His research interests include the design, fabrication, and characterization of high-speed optoelectronic and microwave electronic devices and circuits for fiber optic and wireless communications, as well as ultrafast analog and digital signal processing.

Dr. Fay is a member of the IEEE Electron Devices Society and the IEEE Microwave Theory and Techniques Society (IEEE MTT-S).

**C. Caneau**, photograph and biography not available at time of publication.

**I. Adesida** (S'75–M'79–SM'84–F'99), photograph and biography not available at time of publication.